Knocking out *ARL13B* completely abolishes primary ciliogenesis in cell lines

Divyanshu Mahajan[1], Hui Min Chia[1], and Lei Lu[1*]

[1]School of Biological Sciences, Nanyang Technological University, 60 Nanyang Drive, Singapore 637551.

*Correspondence should be addressed to:
Lei Lu (PhD)
School of Biological Sciences, Nanyang Technological University, 60 Nanyang Drive, Singapore 637551
Tel: 65-65922591
Email: lulei@ntu.edu.sg

Keywords: ARL13B, cilium, ciliogenesis, hedgehog signaling, Joubert syndrome.

Abstract:

Small G protein ARL13B localizes to the cilium and plays essential roles in cilium biogenesis, organization, trafficking, and signaling. Here, we established multiple ARL13B knockout cell lines using the CRISPR/Cas9 system. Surprisingly, all our cell lines lost their cilia completely, in contrast to the reported short cilium and reduced ciliogenesis phenotype. We found that multiple regions of ARL13B are necessary for a complete rescue. Additionally, we found that ARL13B knockout cells also lost their response to SMO-mediated hedgehog stimulation. Our work demonstrates the critical requirement of ARL13B for ciliogenesis and hedgehog signaling, at least in cultured cells, and suggests that ARL13B plays a more crucial role in ciliary function than previously understood.

Introduction

The primary cilium (hereafter cilium) is a microtubule-based plasma membrane protrusion that functions as the cell's antenna. The cilium detects extracellular signals through cilium-localized receptors and triggers intracellular responses through various signaling pathways, such as hedgehog, Wnt, and TGFβ signal transduction pathways [1-3]. The critical role of the cilium in sensing and transducing signals for development and physiological function depends on its unique proteins, mutations of which can cause human disorders collectively termed ciliopathies [4, 5]. The ARF family small G protein ARL13B, the mutation of which causes the ciliopathy Joubert syndrome, has been recognized as one of the most crucial cilium regulators. ARL13B is highly enriched in the cilium, and such localization was mediated by the ciliary transport adaptor Rab8-TNPO1 or Tulp3 [6, 7]. Within the cilium, ARL13B recruits INPP5E to modulate the level of phosphoinositides [8-11]. ARL13B can also function as a guanine nucleotide exchange factor to activate another cilium-localized ARF family small G protein, ARL3, to transport lipidated cargos to the cilium [12-14].

Deletion of *ARL13B* in animals causes diverse cilium-associated physiological and cellular phenotypes [15-23]. For example, *ARL13B* null zebrafish (*scorpion* mutant) is characterized by cystic kidney and body curvature with significantly reduced cilium number and abnormal cilium organization [17]. *ARL13B* null mice (*hennin* mutant) have defective neural tubes, abnormal eyes, and axial polydactyly. At the molecular and cellular level, *hennin* mutant cells display reduced cilium length and biogenesis, abnormal cilium organization, and defective hedgehog signaling [16, 20]. With the advent of CRISPR/Cas9 technology, the *ARL13B* gene has been targeted to generate knockout (KO) cell lines. *ARL13B*-KO hTert-RPE1 (hereafter RPE1) and IMCD3 cells display short cilium with reduced ciliogenesis, consistent with observations in *ARL13B* null animals [9, 24]. In this work, we produced *ARL13B*-KO RPE1 and HEK293T cells and confirmed the KO of *ARL13B* by genotyping and Western blotting. Surprisingly, we found that cilia were completely lost in our *ARL13B*-KO cells. Concomitantly, the hedgehog signaling was abolished in these cells. Therefore, our data demonstrate that ARL13B might play a more critical role in cilium biogenesis and hedgehog signaling than previously recognized.

Result

ARL13B-KO RPE1 cells completely lack cilia.

To study the cellular function of ARL13B, we employed CRISPR/Cas9-induced frameshift mutation to KO the *ARL13B* gene in RPE1 cells. We designed two sgRNAs, sg1 and 2, to target exons 1 and 5 of the human *ARL13B* gene, respectively (Fig. 1a). After lentivirus-mediated transduction of a single expression vector containing the sgRNA and Cas9, RPE1 cells were subjected to puromycin selection. We selected two stable cell lines, sg1#a and sg2#4, corresponding to sg1 and sg2, respectively. We sequenced the genomic DNA fragments containing the sgRNA target sites from sg1#a and sg2#4 cell lines. We found that the two cell lines have frameshift insertion or deletion of nucleotides in both alleles, which were expected to cause a premature translation termination of the transcribed mRNA and trigger the non-sense-mediated mRNA decay [25]. The open reading frames of frameshifted *ARL13B* in sg1#a and sg2#4 cell lines contain less than 13 and 169 AAs (Supplementary File 1), respectively, compared to wild type (WT) ARL13B, 428 AAs. Next, we assessed ARL13B protein levels in cell lysates prepared from sg1#a and sg2#4 cell lines using Western blotting. A single band at the expected molecular weight of ~ 48 kDa was observed in parental RPE1 cells. In contrast, no band was observed in the two KO cell lines (Fig. 1b), supporting that sg1#a and sg2#4 are *ARL13B*-KO cells.

Serum starvation dramatically increased the ciliogenesis percentage of parental RPE1 cells from ~ 20% to 70%, as revealed by immunostaining endogenous ARL13B, acetylated tubulin, or glutamylated tubulin (Fig. 1c,d), which are conventional cilium markers. Our immunofluorescence staining confirmed that the endogenous ARL13B level was undetectable in sg1#a and sg2#4 cells, as expected for *ARL13B*-KO. Surprisingly, we found no cilia in our two *ARL13B*-KO cell lines by the acetylated or glutamylated tubulin immunostaining. Our measured ciliogenesis percentages are 0.0 ± 0.0 % (*mean* ± *standard deviation* and same for the rest of the manuscript) (n = 3) in the two KO cell lines stained by the two tubulin cilium markers. Due to their possible short length and weak intensity, many acetylated or glutamylated tubulin-positive cilia might not be identified unambiguously against the cellular background in RPE1 cells. To facilitate the identification of cilia, we co-labeled the cilium and its base by immunostaining endogenous glutamylated tubulin and pericentrin [26] (Fig. 1e). In parental RPE1 cells, the cilium marked by glutamylated tubulin always extended from the cilium base marked by pericentrin-positive puncta. In contrast, we never observed cilia around the pericentrin puncta in sg1#a and sg2#4 cells. We also employed another cilium marker, fibrocystin ciliary targeting signal (CTS)-fused CD8a (CD8a-fCTS) [27] (Supplementary Fig. 1a, b), and we could not find cilia in our *ARL13B*-KO cell lines either. In summary, our data shows that *ARL13B*-KO RPE1 cells completely lack cilia.

To confirm that the no-cilium phenotype is not an off-target effect of gene editing, we performed rescue experiments by exogenously expressing CRISPR/Cas9-resistant ARL13B coding sequence ($ARL13B^R$). $ARL13B^R$ was constructed by making multiple silent point mutations within sg1 and sg2 target sites in the coding sequence of ARL13B (Fig. 1f). After the lentivirus-transduction of $ARL13B^R$-GFP, sg1#a and sg2#4 cells were subjected to serum starvation and immunostaining of endogenous acetylated tubulin (Fig. 1g). Among GFP-positive cells, we observed 65 ± 3 % (n = 3) and 67 ± 2 % (n = 3), respectively, had cilia (Fig. 1h; Supplementary Fig. 1c). The ciliogenesis percentages of rescued cells had no significant difference from that of parental RPE1 cells (p = 0.001 by unpaired and two-tailed t-test). We previously introduced the cilium to plasma membrane intensity ratio (*CPIR*) as an expression level-independent metric that

quantitatively measures the cilium localization [27]. We found that the *CPIR*s of ARL13B^{R}-GFP and cilium lengths in rescued cells had no significant difference from those of parental RPE1 cells (Fig. 1i, j; Supplementary Fig. 1d, e). Therefore, our study demonstrates that ARL13B^{R}-GFP can rescue the no-cilium phenotype in *ARL13B*-KO cells, suggesting that the no-cilium phenotype should be specific to *ARL13B*-KO.

No cilia could be found in *ARL13B*-KO HEK293T cells either.

We employed HEK293T cell lines to perform similar KO and characterization experiments to confirm our findings in another cell line. We used the same sgRNAs, sg1 and sg2, to generate *ARL13B*-KO cell lines, sg1#5 and sg2#5, respectively. Their genotypes confirmed the frameshift mutations in both alleles (Fig. 2a). By immunofluorescence imaging and Western blotting, we verified that ARL13B protein levels were undetectable in both cell lines (Fig. 2b, c). After serum starvation, we observed 43 ± 4 % (n = 3) parental HEK293T cells acquired acetylated or glutamylated tubulin-positive cilia (Fig. 2d, e). However, under identical treatment, we found no cilia in our two *ARL13B*-KO HEK293T cell lines, in which all ciliogenesis percentages were measured to be 0.0 ± 0.0 % (n = 3). We also demonstrated that the no-cilium phenotype in our *ARL13B*-KO HEK293T cell lines could be rescued by exogenously expressing ARL13B^{R}-GFP (Supplementary Fig. 2). Therefore, our data confirms the no-cilium phenotype upon *ARL13B*-KO in HEK293T cells and suggests that such an observation might apply to multiple types of cells.

***ARL13B*-KO by previously reported sgRNAs also displayed the no-cilium phenotype.**

The no-cilium phenotype we observed in two *ARL13B*-KO cell lines differs from previous studies, such as *ARL13B* null mice (*hennin*) [16, 20] and zebrafish (*scorpion*) [17]. It is especially in stark contrast to a similar work by Nozaki *et al*., who produced *ARL13B*-KO RPE1 cells using CRISPR/Cas9 technique [9]. Nozaki *et al*. reported that cilia were still clearly present in *ARL13B*-KO cells but with a reduced length. To resolve this discrepancy, we adopted the same two sgRNAs they designed, sg4 and sg5, corresponding to sgRNA #1 and #2 in their study, to knock out *ARL13B* gene in the same RPE1 cells. Our effort resulted in two clonal cell lines, sg4#2 and sg5#3, respectively (Fig. 3a). Their frameshift insertion and deletion genotypes and undetectable expression levels of ARL13B in Western blot and immunofluorescence confirmed their ARL13B null phenotypes in both cell lines (Fig. 1b; Fig. 3b). Importantly, consistent with our sg1#a, sg2#4, sg1#5, and sg2#5 cells, we still observed a complete loss of cilia by immunostaining of endogenous acetylated and glutamylated tubulin with a ciliogenesis percentage of 0.0 ± 0.0 % (n = 3) for both cell lines (Fig. 3b, c). Similarly, we also demonstrated that the no-cilium phenotype was rescued by exogenously expressing ARL13B^{R}-GFP (Fig. 3d).

Gene KOs generated by the CRISPR/Cas9-induced frameshift mutation can sometimes still express residual target protein, resulting in a weak phenotype [28-30]. Since our KO cells exhibit a much stronger phenotype, no-cilium, than that reported by Nozaki *et al*. and others, which is reduced cilium length and ciliogenesis percentage [9, 16, 17], we believe our KO cells likely represent a more complete deletion of the *ARL13B* gene (see Discussion). In summary, using two sgRNAs in two cell lines and replicating a previous study, we demonstrated that *ARL13B*-KO cells lack cilia entirely rather than merely exhibiting reduced cilium length and biogenesis.

Multiple ARL13B regions or domains are essential for its ciliogenesis function.

To investigate the roles of different ARL13B regions or domains in ciliogenesis, we assessed the rescue of the no-cilium phenotype of sg1#a cells using a series of ARL13B mutants. ARL13B

144 consists of the following regions or domains from the N to the C-terminus: an α-helix region with
145 palmitoylation lipid anchorage sites (PAL), a GTPase domain, a coiled-coil region (CC), an
146 intrinsically disordered region (IDR), the RVEP motif, and a proline-rich region (PRR) (Fig 4a).
147 The N-terminal PAL contains two palmitoylation sites at C8 and C9, which enable the membrane
148 anchorage of ARL13B. Mutation of both palmitoylation sites from cysteine to serine (C8S/C9S) in
149 PAL abolishes the cilium localization of ARL13B [6, 24, 31, 32]. The GTPase domain is essential
150 for the interaction with INPP5E and can act as a guanine nucleotide exchange factor for ARL3 [8,
151 9, 12-14]. According to the structural and functional analysis of Ras superfamily (including ARF
152 family) small G proteins, the T35N mutation of the GTPase domain's G1 box is expected to lock
153 ARL13B in a GDP-binding state [33-35]. The cellular function of the CC remains elusive, but it is
154 essential for the cilium localization of ARL13B and INPP5E interaction [6, 9]. While the function
155 of the IDR is still unclear, the PRR is known to interact with the IFT-B complex and INPP5E [9].
156 Although both IDR and PRR are dispensable for the cilium localization of ARL13B, the RVEP
157 motif, a stretch of 17 AAs located between the IDR and PRR, serves as the CTS of ARL13B by
158 interacting with ciliary transport adaptors, TNPO1 and Rab8 [6].

159 We prepared the following mutants in the background of ARL13B^{R}-GFP: C8S/C9S, ΔGTPase
160 (deletion of GTPase domain), ΔCC (deletion of CC), ΔIDR (deletion of IDR), RVEP-4A (mutation
161 of RVEP to AAAA), ΔPRR (deletion of PRR), and AA1-245 (deletion of AAs from 246 to 428) (Fig.
162 4a). In parental RPE1 cells, we demonstrated that C8S/C9S and ΔCC do not localize to the cilium,
163 while ΔGTPase, ΔIDR, and ΔPRR show robust cilium localization and RVEP-4A and AA1-245
164 exhibit weak cilium localization (Fig. 4a; Fig. 4b, parental RPE1 cells), consistent with our previous
165 study [6]. Additionally, we observed that T35N has a robust cilium localization (Fig. 4a; Fig. 4b,
166 parental RPE1 cells).

167 Next, we tested these ARL13B mutants for their ability to rescue the no-cilium phenotype of sg1#a
168 cells. Following lentivirus-mediated transduction and serum starvation, we analyzed ciliogenesis
169 by immunostaining endogenous acetylated tubulin and pericentrin (Fig. 4b, c). We found that
170 T35N, ΔIDR, and ΔPRR successfully rescued the no-cilium phenotype with a ciliogenesis
171 percentage of ≥ 70 %, showing no significant difference from ARL13B^{R}-GFP ($p > 0.05$) (Fig. 4c).
172 In contrast, no cilia were found in C8S/C9S, ΔGTPase, ΔCC, and AA1-245 expressing sg1#a
173 cells, all exhibiting a ciliogenesis percentage of 0.0 ± 0.0 % ($n = 3$) (Fig. 4c).

174 Interestingly, although RVEP-4A-expressing sg1#a cells did not show a significant difference (p
175 > 0.05) from WT-expressing cells in terms of the ciliogenesis percentage, 65 ± 3 % vs. 67 ± 2 %
176 ($n = 3$) (Fig. 4d), the resulting cilia were significantly ($p < 0.05$) shorter than WT, measuring 3.3 ±
177 0.6 vs 4.4 ± 0.3 μm, respectively ($n = 3$)(Fig. 4e). Our observation of the RVEP-4A mutant is
178 consistent with a previous study where ARL13B with V358A mutation did not rescue the cilium
179 length in *ARL13B* null *hennin* mouse embryonic fibroblasts [36]. The partial rescue phenotype
180 might be due to the insufficient amount of cilium-localized ARL13B, as revealed by its significantly
181 ($p < 0.05$) lower *CPIR* than WT in parental RPE1 cells, at 0.61 ± 0.04 vs. 8.5 ± 0.5 ($n = 3$),
182 respectively (Fig. 4f). This observation is consistent with previous reports showing that the ciliary
183 level of ARL13B regulates cilium length [20, 37]. In parental RPE1 cells, overexpression of the
184 RVEP-4A mutant also significantly reduced cilium length compared to WT ARL13B, with lengths
185 of 2.5 ± 0.3 μm vs. 4.3 ± 0.4 μm, respectively ($p < 0.005$, $n = 3$) (Fig. 4e). It is possible that
186 overexpression of the RVEP-4A mutant, as demonstrated by our quantitative
187 immunofluorescence imaging (Supplementary Fig. 3), interferes with the ciliary targeting of

endogenous ARL13B in a dominant-negative manner, thereby contributing to the short cilium phenotype.

In summary, we demonstrated that our *ARL13B-KO* cells provided an excellent tool to test the ciliogenesis role of ARL13B domains, motifs, or mutations, as evidenced by the clear contrast with the no-cilium phenotype during the rescue. Our extensive mutagenesis demonstrated that the ciliogenesis function of ARL13B requires the N-terminal palmitoylation, the GTPase domain, and the CC. We found that cilium localization of ARL13B mutants is necessary but insufficient for ciliogenesis, as shown by ΔGTPase and AA1-245. Furthermore, our data on the RVEP-4A mutant suggests that cilium formation requires a minimal amount of ciliary ARL13B, while the dose of cilium-localized ARL13B might be a limiting factor for cilium length.

Joubert syndrome mutation, R200C, abolishes the ciliogenesis function of ARL13B

We focused on the three point mutations in the coding sequence of the *ARL13B* gene, which have been associated with the Joubert syndrome [38, 39]. Among them, R79Q, and Y86C are in the GTPase domain, while R200C is in the CC. To characterize the impact of these point mutations on the ciliogenesis function of ARL13B, we made corresponding mutations in the background of ARL13B^{R}-GFP (Fig. 5a). First, we examined their cilium localization in parental RPE1 cells, similar to our approach with other mutants. We found that R79Q and Y86C had robust cilium localization comparable to WT (Fig. 5b). The cilium localization of R200C was significantly weaker than that of WT (Fig. 5b). Next, we tested if ARL13B with these Joubert syndrome point mutations can rescue the no-cilium phenotype of sg1#a cells (Fig. 5c). Following lentivirus-mediated transduction, serum starvation, and immunostaining, we analyzed the ciliogenesis of these mutants. R79Q and Y86C displayed ciliogenesis percentages of 71 ± 3 % (n = 3) and 73 ± 1 % (n = 3) in sg1#a cells (Fig. 5d), respectively, similar to WT (Fig. 1h). In contrast, no cilia were observed in R200C-expressing sg1#a cells, which exhibited a ciliogenesis percentage of 0.0 ± 0.0 % (n = 3) (Fig. 5d). In summary, our data revealed that R200C completely abolishes the ciliogenesis function of ARL13B, highlighting the essential role of the CC in ciliogenesis and suggesting a cellular mechanism of R200C mutation for the Joubert syndrome pathology. In contrast, the R79Q and Y86C mutations do not appear to impair ciliogenesis, implying that their cellular effects might act downstream of cilium formation.

Hedgehog signaling is abolished in *ARL13B*-KO cells.

It is known that the hedgehog signaling requires the cilium [40]. The stimulation of hedgehog recruits SMO to the cilium and upregulates the transcription of hedgehog signaling target genes, such as *SMO*, *PTCH1*, and *GLI1*. Previous studies established that the loss of ARL13B disrupts the hedgehog signaling in vertebrates such as mouse (*hennin* mutant) and zebrafish (*scorpion* mutant) [16, 17], which have the phenotypes of reduced cilia. Therefore, we want to investigate the impact of a complete cilium loss on the hedgehog signaling pathway in our *ARL13B*-KO cells by assessing the cilium localization of SMO and measuring the transcription of *SMO*, *PTCH1*, and *GLI1* genes.

In serum-starved parental RPE1 cells, we immunostained the endogenous ARL13B and SMO. We observed that only 11 ± 3 % (n = 4) of ciliated cells had the cilium localization of SMO (Fig. 6a, b control). In comparison, after 24 h treatment with 0.5 μM SAG (SMO agonist), a small molecule that directly activates SMO, the cilium localization of SMO significantly (p < 0.005)

231 increased to 75 ± 5 % (*n* = 4) in ciliated cells (Fig. 6a, b). Using qPCR, we found that SAG
232 treatment after serum starvation increased the normalized transcription levels of *SMO*, *PTCH1*,
233 and *GLI1* genes to 2.3 ± 0.9, 1.6 ± 0.3, and 4.5 ± 3.6, respectively, (*n* = 5, normalized by control),
234 respectively (Fig. 6c). Our results are consistent with what we know about the SMO-activated
235 hedgehog signaling, thereby validating our assay setup.

236 Since *ARL13B*-KO sg1#a cells have no cilia, hedgehog signaling components, including SMO,
237 could not localize to the cilium. To assess the hedgehog signaling upon the KO of *ARL13B*, we
238 quantified the hedgehog-dependent transcription of *SMO*, *PTCH1*, and *GLI1* genes. First, we
239 found no significant difference in the transcript levels of *SMO*, *PTCH1*, and *GLI1* genes between
240 parental RPE1 and sg1#a cells (Supplementary Fig. 4). Next, we treated sg1#a and parental
241 RPE1 cells in parallel with serum-starvation followed by SAG, as described in Figure 6c. In
242 contrast to the parental RPE1 cells, we found that SAG treatment did not increase the relative
243 transcription levels of *SMO*, *PTCH1*, and *GLI1* genes; instead, it slightly reduced their levels to
244 0.7 ± 0.1, 0.7 ± 0.5, and 0.7 ± 0.2, respectively, (*n* = 5, normalized by untreated). Among these,
245 the reductions in *SMO* and *GLI1* transcription were statistically significant, whereas the change in
246 *PTCH1* was not. The biological significance of the decreased transcription of *SMO* and *GLI1*
247 remains unclear and warrants further investigation.

248 The exogenous expression of ARL13B^{R}-GFP rescued the SAG-induced cilium localization of
249 SMO in sg1#a cells, as we observed an increase in the cilium localization of SMO among GFP-
250 positive ciliated cells from 0 % to 56 ± 5 % (*n* = 3) following SAG treatment (Fig. 6d,e),
251 demonstrating that the observed effect on hedgehog signaling is specific to *ARL13B*-KO. In
252 summary, our results revealed that hedgehog signaling is severely blunted upon the KO of
253 *ARL13B*, suggesting that *ARL13B*-KO cells might become irresponsive to hedgehog.

Discussion

ARL13B null mice and zebrafish have been reported previously to display a reduced but still appreciable ciliogenesis percentage, cilium length, and hedgehog signaling. Similarly, *ARL13B*-KO RPE1 and IMCD3 cells have been shown to form cilia, albeit with reduced length [9, 24]. However, our *ARL13B*-KO cells, generated using four sgRNAs in two cell types, RPE1 and HEK293T, consistently exhibited much more extreme phenotypes — both cilia and hedgehog signaling appear to be completely lost, which is in stark contrast to many previous studies. Despite using the same cell type (RPE1) and technique (CRISPR/Cas9), our findings differ significantly from those of Nozaki et al., as we observed a non-cilium phenotype even after adopting the same sgRNAs. However, our results are supported by those of Shi *et al.*, who reported cilia loss in *ARL13B*-KO glioma cell lines generated using CRISPR/Cas9 [41], and by Li *et al.*, who observed the absence of cilia in specific kidney cell types following *ARL13B* deletion via the Cre-LoxP system in mice [21].

It has recently been reported that KO clones generated by CRISPR/Cas9-induced frameshift often express a residual amount of the target protein and, therefore, can produce much milder phenotypes than expected [28-30]. The low expression of the target protein in these “pseudo-KO” clones could result from multiple mechanisms, such as alternative splicing or usage of the downstream start codon of the target mRNA. Thus, it is tempting to speculate that *ARL13B*-KO clones and null mutants generated by Nozaki *et al*. and other labs could be such cases with a low level of ARL13B protein but still sufficient to support ciliogenesis. Hence, their phenotypes are weaker than ours. Supporting this hypothesis, we found that reducing the ciliary localization of ARL13B by mutating its CTS, the RVEP motif, did not affect ciliogenesis but significantly shortened the cilium length (Fig. 4e). To confirm this hypothesis, we propose three possible experiments using these “pseudo-KO” cells. First, the residual amount of the target protein can be enriched and subjected to a more sensitive Western blotting assay. Second, reverse transcription PCR can be employed to detect alternative splicing events of the *ARL13B* mRNA. Lastly, further knockdown of ARL13B by RNAi in these cells should produce no-cilium phenotypes similar to ours.

Our data revealed the crucial requirement of ARL13B in ciliogenesis. Our rescue experiments in *ARL13B*-KO cells using ARL13B mutants further suggest the roles of different ARL13B regions and domains in ciliogenesis. The palmitoylation membrane anchorage, the GTPase domain, and the CC, but not the IDR and PRR, are required for ciliogenesis. In addition, the guanine nucleotide exchange of ARL13B might not be required, as suggested by the GDP-locked mutation, T35N. The RVEP motif regulates the ciliary localization of ARL13B, which is essential for cilium growth. Mutation of this motif, as in RVEP-4A, impairs ARL13B targeting to the cilium and results in a short-cilium phenotype (Fig. 4e). Additionally, we examined three Joubert syndrome point mutations and found that R200C, but not R79Q and Y86C, abolished the ciliogenesis. Therefore, our data also help us to understand the pathogenesis of Joubert syndrome with R200C mutation.

292 **Material and methods:**

293 **DNA plasmids**

294 Please see Supplementary Table 1 for all the plasmids used in this study. pLenti-CRISPR v2 was
295 a gift from Feng Zhang (Addgene plasmid # 52961; http://n2t.net/addgene:52961; RRID:
296 Addgene_52961).

297 **Antibodies**

298 Mouse monoclonal antibodies (mAbs) against acetylated α-tubulin (Merck, #T6793, 1:1000 for
299 immunofluorescence or IF), polyglutamylated tubulin (Adipogen, #GT335, 1:1000 for IF), CD8a
300 (Developmental Studies Hybridoma Bank, clone OKT8, 1:200 for IF), GAPDH (Santa Cruz,
301 #sc25778, 1:1000 for WB), and SMO (Santa Cruz, #sc-166685) Rabbit polyclonal antibodies
302 (pAbs) against ARL13B (in-house made; 1:1000 for IF)[27], ARL13B (ProteinTech, #17711-AP,
303 1:1000 for IF and 1:3000 for WB), and pericentrin (Abcam, #ab4448, 1:1000 for IF). Horseradish
304 peroxidase (HRP) -conjugated goat anti-mouse and anti-rabbit IgG antibodies were purchased
305 from Bio-Rad. Alexa Fluor-conjugated goat anti-mouse and anti-rabbit IgG antibodies (1:500 for
306 IF) were purchased from Invitrogen.

307 **Cell culture and transfection**

308 hTert-RPE1 and HEK293T cells were from the American Type Culture Collection. 293FT cells
309 were from Thermo Fisher Scientific. RPE1 cells were cultured in Dulbecco's Modified Eagle's
310 Medium (DMEM) and Ham's F12 mixture medium supplemented with 10% fetal bovine serum
311 (FBS). HEK293T cells were cultured in DMEM supplemented with 10% FBS. 293FT were cultured
312 in DMEM supplemented with 10% FBS and 500 µg/ml Geneticin™ (Thermo Fisher Scientific,
313 #10131035). Transfection of plasmid DNA was performed using polyethylenimine (Polysciences)
314 or Lipofectamine 2000 (Thermo Fisher Scientific, #11668019), according to the manufacturer's
315 protocol. Ciliogenesis was induced by incubating cells in the corresponding medium without the
316 FBS for 48 h (serum starvation).

317 **Lentivirus-transduced KO and rescue of *ARL13B***

318 sgRNA cloned in pLenti-CRISPRV2 vector or ARL13B^{R} WT and mutants cloned in pLVX-puro
319 vector were transiently transfected with packaging plasmids pLP1, pLP2, and pLP/VSVG (Thermo
320 Fisher Scientific) to 293FT cells using Lipofectamine 2000 according to the manufacturer's
321 protocol. Lentiviruses were harvested 36 and 60 h post-transfection, filtered through a 0.45 µm
322 syringe-driven filter (Sartorius), and immediately used to infect WT RPE1, HEK293T, or *ARL13B*-
323 KO cell lines.

324 To make *ARL13B*-KO cell lines, RPE1 or HEK293T cells seeded in a 6-well plate were infected
325 twice every 24 h with filtered lentiviruses using 8 µg/ml hexadimethrine bromide (Sigma-Aldrich,
326 #H9268). 24 h after the second infection, the cells were then selected in media supplemented
327 with 8 and 1 µg/ml puromycin (Sigma-Aldrich, #P8833) for 72 h for RPE1 and HEK293T cells,
328 respectively. Subsequently, highly diluted cells were seeded into a 96-well plate so that each well
329 had at most one colony. Colonies were harvested, expanded, and characterized for *ARL13B*-KO
330 using immunofluorescence and Western blotting. At least one clonally selected cell line for each
331 sgRNA was selected and sequenced around the sgRNA target site to confirm frameshift
332 mutations in both.

333 In rescue experiments, *ARL13B*-KO cells seeded in a 6-well plate were infected twice every 24 h
334 with filtered lentiviruses using 8 μg/ml hexadimethrine bromide. The cells were then seeded into
335 a 24-well plate containing coverslips for immunofluorescence followed by serum starvation for 48
336 h to induce ciliogenesis before immunolabeling. For the hedgehog signaling assay, 24 h treatment
337 with 0.5 μM SAG (Abcam, #ab142160) was performed before immunolabeling.

338 **Western blot**

339 Parental and *ARL13B-KO* cells seeded in a 6-well plate were lysed in the SDS sample buffer and
340 resolved in SDS-PAGE. SDS-PAGE separated proteins were transferred to polyvinyl difluoride
341 membrane (Bio-Rad), which was sequentially incubated with primary and HRP-conjugated
342 secondary antibody. Western blot and molecular weight marker bands were acquired under the
343 chemiluminescence and white-light imaging mode, respectively, using a cooled charge-coupled
344 device of LAS-4000 (GE Healthcare Life Sciences). Molecular weights were manually assigned
345 by aligning the two images. Uncropped blot images are presented in Supplementary Fig. 5.

346 **RT-qPCR for SAG-activated hedgehog signaling pathway**

347 RPE1 and *ARL13B*-KO cells were cultured to confluence in a 6-well plate, followed by serum
348 starvation for 48 h to induce ciliogenesis. After 48 h of starvation, the control sample was cultured
349 for another 24 h in the serum starvation medium, and the SAG sample was subjected to 0.5 μM
350 SAG. Total RNA was extracted using TRIzol™ Reagent (Invitrogen™, #15596025) and reverse-
351 transcribed, primed by random nonamer primers using M-MuLV Reverse Transcriptase (NEB,
352 #M0253), following the manufacturer's standard protocol. The qPCR reactions were performed
353 using the iTaq Universal SYBR Green Supermix (Bio-Rad, #1725121), in accordance with the
354 manufacturer's instructions. Gene expression data for β actin, *SMO*, *PTCH1,* and *GLI1* were
355 acquired using Bio-Rad CFX Connect Real-Time PCR Detection System. The qPCR result of
356 each gene was first divided by that of β actin and further normalized to that of control. The relative
357 gene expression was calculated through $2^{-\Delta\Delta CT}$ method. Primer designed for the target genes are
358 listed in Supplementary Table 1.

359 **Immunolabeling and wide-field fluorescence microscopy**

360 RPE1 and HEK293T cells were first seeded on No. 1.5 Φ 12-mm coverslips in a 24-well plate.
361 Next, cells were serum starved for 48 h to induce ciliogenesis, fixed with 4% paraformaldehyde
362 in PBS, and subsequently neutralized with ammonium chloride. Subsequently, the cells were
363 incubated with primary antibodies diluted in the antibody dilution buffer, which consists of PBS
364 supplemented with 5% FBS, 2% bovine serum albumin, and 0.1% Saponin (Sigma-Aldrich). After
365 several washings, cells were incubated with secondary antibodies diluted in the antibody dilution
366 buffer. The coverslips were mounted in Mowiol 4-88 (EMD Millipore) after extensive washing
367 using PBS. Finally, cells were imaged under an inverted wide-field Olympus IX83 microscope
368 system equipped with a Plan Apo oil objective lens (63×, NA 1.40), a motorized stage, a focus
369 drift correction device, motorized filter cubes, a scientific complementary metal oxide
370 semiconductor camera (Neo; Andor Technology), and a 200 W metal halide excitation light source
371 (Lumen Pro 200; Prior Scientific). Dichroic mirrors and filters in filter turrets were optimized for
372 Alexa Fluor 488 (or GFP), Alexa Fluor 594, and Alexa Fluor 680. The microscope system was
373 controlled by MetaMorph software 7.8.3.0 (Molecular Devices,
374 https://support.moleculardevices.com/s/article/MetaMorph-Software-installation-files).

375 **Image analysis for the ciliogenesis percentage, the cilium length, and the *CPIR***

Untransfected cells were serum-starved to induce ciliogenesis. They were subsequently fixed and subjected to immunofluorescence labeling for endogenous cilium markers before wide-field microscopy imaging. The ciliogenesis percentage was calculated by dividing the number of ciliated cells by the total number of analyzed cells. Parental or *ARL13B*-KO cells expressing ARL13B^{R}-GFP WT and mutants were similarly processed and imaged. Their ciliogenesis percentages were calculated by dividing the number of ciliated GFP-positive cells by the total number of analyzed GFP-positive cells. The cilium length and the *CPIR* of ARL13B^{R}-GFP WT or mutant were measured in ciliated GFP-positive cells using Fiji version 1.54d (https://fiji.sc/). To calculate cilium length, the cilium was traced by a line, and the length of the line was measured in Fiji. The calculation of the *CPIR* was performed as described previously [27]. Briefly, first, a ~1 μm thick line was drawn orthogonally across the cilium in Fiji. Next, the line intensity profile of the cilium was determined, and the maximum intensity value (I_{max}) was obtained. Similarly, by drawing a circular ROI (region of interest) on the PM and the background region, the mean intensity of PM (I_{PM}) and the background value ($I_{background}$) were acquired, respectively. Finally, the CPIR of ARL13B^{R}-GFP WT or mutant was calculated as $(I_{max} - I_{PM})/(I_{PM} - I_{background})$.

Data analysis and graphs were plotted using OriginPro version 9.9 (OriginLab, https://www.originlab.com). The sample size *n* is indicated wherever applicable in figures or corresponding legends. Data are presented as the *mean ± standard deviation (s.d.)*. The two-tailed unpaired *t*-test was conducted in Excel (Microsoft, https://www.microsoft.com/en-us/microsoft-365/excel). A *p*-value ≤ 0.05 was considered statistically significant.

396 **References:**

397 1. Anvarian, Z., et al., *Cellular signalling by primary cilia in development, organ function and*
398 *disease.* Nat Rev Nephrol, 2019. **15**(4): p. 199-219.
399 2. Wheway, G., L. Nazlamova, and J.T. Hancock, *Signaling through the Primary Cilium.* Frontiers in
400 Cell and Developmental Biology, 2018. **6**(8).
401 3. Pala, R., N. Alomari, and S.M. Nauli, *Primary cilium-dependent signaling mechanisms.*
402 International journal of molecular sciences, 2017. **18**(11): p. 2272.
403 4. Hildebrandt, F., T. Benzing, and N. Katsanis, *Ciliopathies.* New England Journal of Medicine,
404 2011. **364**(16): p. 1533-1543.
405 5. Goetz, S.C. and K.V. Anderson, *The primary cilium: a signalling centre during vertebrate*
406 *development.* Nature Reviews Genetics, 2010. **11**(5): p. 331-344.
407 6. Mahajan, D., V. Madugula, and L. Lu, *Rab8 and TNPO1 are ciliary transport adaptors for GTPase*
408 *Arl13b by interacting with its RVEP motif containing ciliary targeting sequence.* J Biol Chem,
409 2023. **299**(5): p. 104604.
410 7. Palicharla, V.R., et al., *Interactions between TULP3 tubby domain and ARL13B amphipathic helix*
411 *promote lipidated protein transport to cilia.* Mol Biol Cell, 2023. **34**(3): p. ar18.
412 8. Humbert, M.C., et al., *ARL13B, PDE6D, and CEP164 form a functional network for INPP5E ciliary*
413 *targeting.* Proc Natl Acad Sci U S A, 2012. **109**(48): p. 19691-6.
414 9. Nozaki, S., et al., *Regulation of ciliary retrograde protein trafficking by the Joubert syndrome*
415 *proteins ARL13B and INPP5E.* J Cell Sci, 2017. **130**(3): p. 563-576.
416 10. Chavez, M., et al., *Modulation of Ciliary Phosphoinositide Content Regulates Trafficking and*
417 *Sonic Hedgehog Signaling Output.* Dev Cell, 2015. **34**(3): p. 338-50.
418 11. Garcia-Gonzalo, F.R., et al., *Phosphoinositides Regulate Ciliary Protein Trafficking to Modulate*
419 *Hedgehog Signaling.* Dev Cell, 2015. **34**(4): p. 400-409.
420 12. Gotthardt, K., et al., *A G-protein activation cascade from Arl13B to Arl3 and implications for*
421 *ciliary targeting of lipidated proteins.* Elife, 2015. **4**.
422 13. Ivanova, A.A., et al., *Biochemical characterization of purified mammalian ARL13B protein*
423 *indicates that it is an atypical GTPase and ARL3 guanine nucleotide exchange factor (GEF).* J Biol
424 Chem, 2017. **292**(26): p. 11091-11108.
425 14. Zhang, Q., et al., *GTP-binding of ARL-3 is activated by ARL-13 as a GEF and stabilized by UNC-*
426 *119.* Sci Rep, 2016. **6**: p. 24534.
427 15. Augiere, C., et al., *ARL13B controls male reproductive tract physiology through primary and*
428 *Motile Cilia.* Commun Biol, 2024. **7**(1): p. 1318.
429 16. Caspary, T., C.E. Larkins, and K.V. Anderson, *The graded response to Sonic Hedgehog depends on*
430 *cilia architecture.* Dev Cell, 2007. **12**(5): p. 767-78.
431 17. Duldulao, N.A., S. Lee, and Z. Sun, *Cilia localization is essential for in vivo functions of the Joubert*
432 *syndrome protein Arl13b/Scorpion.* Development, 2009. **136**(23): p. 4033-42.
433 18. Hanke-Gogokhia, C., et al., *The guanine nucleotide exchange factor Arf-like protein 13b is*
434 *essential for assembly of the mouse photoreceptor transition zone and outer segment.* J Biol
435 Chem, 2017. **292**(52): p. 21442-21456.
436 19. Higginbotham, H., et al., *Arl13b in primary cilia regulates the migration and placement of*
437 *interneurons in the developing cerebral cortex.* Dev Cell, 2012. **23**(5): p. 925-38.
438 20. Larkins, C.E., et al., *Arl13b regulates ciliogenesis and the dynamic localization of Shh signaling*
439 *proteins.* Mol Biol Cell, 2011. **22**(23): p. 4694-703.
440 21. Li, Y., et al., *Deletion of ADP Ribosylation Factor-Like GTPase 13B Leads to Kidney Cysts.* J Am Soc
441 Nephrol, 2016. **27**(12): p. 3628-3638.

442 22. Seixas, C., et al., *Arl13b and the exocyst interact synergistically in ciliogenesis.* Mol Biol Cell,
443 2016. **27**(2): p. 308-20.
444 23. Su, C.Y., et al., *Temporal deletion of Arl13b reveals that a mispatterned neural tube corrects cell*
445 *fate over time.* Development, 2012. **139**(21): p. 4062-71.
446 24. Roy, K., et al., *Palmitoylation of the ciliary GTPase ARL13b is necessary for its stability and its role*
447 *in cilia formation.* J Biol Chem, 2017. **292**(43): p. 17703-17717.
448 25. Kurosaki, T., M.W. Popp, and L.E. Maquat, *Quality and quantity control of gene expression by*
449 *nonsense-mediated mRNA decay.* Nat Rev Mol Cell Biol, 2019. **20**(7): p. 406-420.
450 26. Jurczyk, A., et al., *Pericentrin forms a complex with intraflagellar transport proteins and*
451 *polycystin-2 and is required for primary cilia assembly.* J Cell Biol, 2004. **166**(5): p. 637-43.
452 27. Madugula, V. and L. Lu, *A ternary complex comprising transportin1, Rab8 and the ciliary*
453 *targeting signal directs proteins to ciliary membranes.* Journal of cell science, 2016. **129**(20): p.
454 3922-3934.
455 28. Smits, A.H., et al., *Biological plasticity rescues target activity in CRISPR knock outs.* Nat Methods,
456 2019. **16**(11): p. 1087-1093.
457 29. Meraldi, P., *Bub1-the zombie protein that CRISPR cannot kill.* EMBO J, 2019. **38**(7).
458 30. Zhang, G., et al., *Efficient mitotic checkpoint signaling depends on integrated activities of Bub1*
459 *and the RZZ complex.* EMBO J, 2019. **38**(7).
460 31. Cevik, S., et al., *Joubert syndrome Arl13b functions at ciliary membranes and stabilizes protein*
461 *transport in Caenorhabditis elegans.* J Cell Biol, 2010. **188**(6): p. 953-69.
462 32. Cevik, S., et al., *Active transport and diffusion barriers restrict Joubert Syndrome-associated*
463 *ARL13B/ARL-13 to an Inv-like ciliary membrane subdomain.* PLoS Genet, 2013. **9**(12): p.
464 e1003977.
465 33. Feig, L.A., *Tools of the trade: use of dominant-inhibitory mutants of Ras-family GTPases.* Nat Cell
466 Biol, 1999. **1**(2): p. E25-7.
467 34. Sztul, E., et al., *ARF GTPases and their GEFs and GAPs: concepts and challenges.* Mol Biol Cell,
468 2019. **30**(11): p. 1249-1271.
469 35. Sprang, S.R., *G protein mechanisms: insights from structural analysis.* Annu Rev Biochem, 1997.
470 **66**: p. 639-78.
471 36. Mariani, L.E., et al., *Arl13b regulates Shh signaling from both inside and outside the cilium.* Mol
472 Biol Cell, 2016.
473 37. Lu, H., et al., *A function for the Joubert syndrome protein Arl13b in ciliary membrane extension*
474 *and ciliary length regulation.* Dev Biol, 2015. **397**(2): p. 225-36.
475 38. Cantagrel, V., et al., *Mutations in the cilia gene ARL13B lead to the classical form of Joubert*
476 *syndrome.* The American Journal of Human Genetics, 2008. **83**(2): p. 170-179.
477 39. Thomas, S., et al., *Identification of a novel ARL13B variant in a Joubert syndrome-affected*
478 *patient with retinal impairment and obesity.* Eur J Hum Genet, 2015. **23**(5): p. 621-7.
479 40. Bangs, F. and K.V. Anderson, *Primary Cilia and Mammalian Hedgehog Signaling.* Cold Spring
480 Harb Perspect Biol, 2017. **9**(5).
481 41. Shi, P., et al., *HDAC6 Signaling at Primary Cilia Promotes Proliferation and Restricts*
482 *Differentiation of Glioma Cells.* Cancers (Basel), 2021. **13**(7).

483

Acknowledgments

We would like to thank the following Feng Zhang (Massachusetts Institute of Technology, USA) for sharing the DNA plasmid (pLenti-CRISPR v2) with us.

Author contributions

L. L. and D. M. conceptualization; D. M., H. M. C., and L. L. methodology; D. M. and H. M. C. analysis, investigation, and validation; D. M. and L. L. writing; L. L. supervision, project administration, and funding acquisition.

Data availability

The datasets generated during the current study are available in the GenBank repository [PV240348 to 359] and are included in Supplementary File 2. The datasets are available from the corresponding author on request.

Supplementary Information

This article contains supporting information.

Competing interests

The authors declare that they have no conflicts of interest with the contents of this article.

Abbreviations

The abbreviations used are listed below: AA, amino acid; CC, coiled-coil region; *CPIR*, the cilium to plasma membrane intensity ratio; IDR, intrinsically disordered region; KO, knock out; NS, not significant; PAL, palmitoylation lipid anchorage site; PTCH1, patched1; PRR, proline-rich region; sgRNA, single guide RNA; SMO, smoothened; WT, wild type.

Funding

This project is supported by the Ministry of Education, Singapore, under its Tier 1 RG 25/22.

512 **Figure Legends**

513 **Figure 1**

514 ***ARL13B*-KO RPE1 cells have no cilia. (a)** A schematic diagram of CRISPR/Cas9 strategy to
515 make frameshift mutations in human *ARL13B* gene. The scheme of the exon organization of the
516 human *ARL13B* gene is illustrated at the top. The middle shows parts of the WT genomic
517 sequences of exon 1 and exon 5, where sequences of two sgRNAs, sg1 and sg2, are highlighted
518 in light blue. Underlined sequences are protospacer-adjacent motifs or PAMs. The bottom shows
519 genomic sequences at sgRNA target sites of two alleles in sg1#a and sg2#4 cell lines. Sequences
520 are aligned with the corresponding WT ones. Inserted and deleted bases are colored red and
521 indicated by "-", respectively. "+2" and "-7" indicate insertion of 2 and deletion of 7 bases,
522 respectively. **(b)** Western blotting of endogenous ARL13B in parental and KO RPE1 cells. Cell
523 lysates from indicated cell lines were subjected to 12% SDS-PAGE followed by immunoblotting
524 using anti-ARL13B and anti-glyceraldehyde 3-phosphate dehydrogenase (GAPDH) (loading
525 control) antibodies. Molecular weight markers are labeled to the right of the immunoblot. **(c)**
526 Fluorescence imaging of endogenous ARL13B and acetylated tubulin in parental and KO RPE1
527 cells. Indicated cells were fixed and co-immunostained by antibodies against indicated cilium
528 markers before being subjected to wide-field microscopy. (**d**) Quantification of the ciliogenesis
529 percentage in parental and KO RPE1 cells. Images acquired as described in (c) were analyzed.
530 n = 3 independent experiments with ≥ 100 cells analyzed in each case. (**e**) Fluorescence imaging
531 of endogenous glutamylated tubulin and pericentrin in parental and KO RPE1 cells, similar to (c).
532 (**f**) Silent mutations in ARL13B^R-GFP make it resistant to sgRNAs. Regions of the ARL13B^R
533 coding sequence, corresponding to sg1, sg2, sg4, and sg5 (colored blue), are shown with
534 introduced multiple silent mutations colored red. Protospacer-adjacent motifs, or PAMs, are
535 underlined. Superscript numbers indicate base pair positions in the coding sequence. (**g**)
536 ARL13B^R-GFP can rescue the no-cilium phenotype of *ARL13B*-KO cell lines. Parental RPE1,
537 sg1#a, and sg2#4 cells expressing ARL13B^R-GFP were processed for immunofluorescence to
538 label endogenous acetylated tubulin and pericentrin. Arrows indicate ciliated cells. In (c, e, and
539 g), the boxed region is enlarged at the lower left corner, and the scale bar represents 10 μm. (**h-**
540 **j**) ARL13B^R-GFP expressing sg1#a cells exhibit normal cilia. Images acquired as described in (g)
541 were used for quantification. Cilia were identified by acetylated tubulin. Panel h shows the
542 ciliogenesis percentage in GFP-positive parental and sg1#a cells (indicated by "+"). It also
543 displays the ciliogenesis percentage of GFP-negative sg1#a cells from the same coverslips
544 (indicated by "-"). Quantification was from n = 3 independent experiments with ≥ 100 cells
545 analyzed in each experiment. In (i), the cilium length was measured in ciliated GFP-positive cells.
546 Quantification was from n = 3 independent experiments with ≥ 30 cells analyzed in each
547 experiment. In (j), the *CPIR* of ARL13B^R-GFP was quantified in ciliated GFP-positive cells.
548 Quantification was from n = 3 independent experiments with ≥ 30 cells analyzed in each
549 experiment. In (d, h-j), the error bar represents the *mean ± standard deviation*.

550

551 **Figure 2**

552 ***ARL13B*-KO HEK293T cells have no cilia. (a)** The genotypes of *ARL13B*-KO HEK293T cell
553 lines, sg1#5 and sg2#5. See the legend of Figure 1a. (**b-e**) Endogenous ARL13B is undetectable
554 by Western blot and immunofluorescence imaging, and no cilia could be found in sg1#5 and
555 sg2#5 cells. In (**b**), anti-GAPDH was used for loading control. Non-specific bands are indicated

556 by asterisks (*). Molecular weight markers are labeled to the right of the immunoblot. See the
557 legend of Figure 1b. (**c**) Fluorescence imaging of endogenous ARL13B and acetylated tubulin in
558 parental and KO HEK293T cells. Cells were fixed and co-immunostained by antibodies against
559 indicated cilium markers before being subjected to wide-field microscopy. (**d**) Quantification of the
560 ciliogenesis percentage in parental and KO HEK293T cells. Images acquired as described in (c)
561 were analyzed. n = 3 independent experiments with ≥ 100 cells analyzed in each case. The error
562 bar represents the *mean* ± *standard deviation*. (**e**) Fluorescence imaging of endogenous
563 glutamylated tubulin and pericentrin in parental and KO HEK293T cells, similar to (c). In (c and
564 e), the boxed region is enlarged at the lower left corner, and the scale bar represents 10 μm.

565

566 **Figure 3**

567 ***ARL13B*-KO RPE1 cells prepared using previously reported sgRNAs have no cilia either.**
568 (**a**) The genotypes of *ARL13B*-KO RPE1 cell lines, sg4#2 and sg5#3, using previously published
569 sgRNAs. See the legend of Figure 1a. (**b-c**) Endogenous ARL13B is undetectable by
570 immunofluorescence imaging and no cilia could be found in sg4#2 and sg5#3 cells. See the
571 legend of Figure 1c, e (**d**) Exogenously expressed ARL13B^{R}-GFP can rescue the no-cilium
572 phenotype of sg4#2 and sg5#3 cells. See the legend of Figure 1g. In (b-d), the boxed region is
573 enlarged at the lower left corner, and the scale bar represents 10 μm.

574

575 **Figure 4**

576 **Multiple ARL13B regions or domains are required for ciliogenesis.** (**a**) The schematic
577 diagram illustrating the organization of WT and mutant ARL13B, which were constructed in the
578 background of ARL13B^{R}-GFP. The top shows the WT ARL13B. Different functional regions and
579 domains are indicated with AA positions. Interacting proteins previously reported are labeled
580 above the corresponding regions or domains and shaded green. The AA sequences of PAL and
581 RVEP motifs are shown below. ARL13B mutants with point mutations or truncations are illustrated
582 below the WT. On the right is the qualitative summary of the cilium localization of corresponding
583 GFP-tagged WT and mutant ARL13B (see below for details). "+" indicates a positive cilium
584 localization; "-" indicates a negative cilium localization or no ciliogenesis; "W" indicates a weak
585 cilium localization. (**b**) The cellular distribution of GFP-tagged WT and mutant ARL13B^{R}-GFP.
586 Parental and sg1#a RPE1 cells expressing GFP-tagged WT and mutant ARL13B^{R}-GFP were
587 immunostained for indicated proteins. The boxed region is enlarged at the lower left corner, and
588 the scale bar represents 10 μm. (**c**) The cilium localization percentage (Parental RPE1 cells) and
589 cilium biogenesis percentage (sg1#a RPE1 cells) of GFP-positive cells. The images acquired as
590 described in (b) were analyzed. n = 3 independent experiments with ≥ 100 cells analyzed in each.
591 (**d-f**) The RVEP motif is non-essential for ciliogenesis but essential for the cilium length and the
592 cilium enrichment of ARL13B^{R}-GFP in *ARL13B*-KO cells. Images acquired as described in (b)
593 were quantified. GFP-positive cells were analyzed for the ciliogenesis percentage (**d**), the cilium
594 length (**e**), and the *CPIR* (**f**) of ARL13B^{R}-GFP. See legend of Figure 1h-j. p-values are from
595 unpaired, two-tailed t-tests. Not significant or NS, $p > 0.05$; ∗, $p \leq 0.05$; ∗∗, $p \leq 0.005$; ∗∗∗, $p \leq$
596 0.0005. In (c, d-f), the error bar represents the *mean* ± *standard deviation.*

597

598 **Figure 5**

599 **Joubert syndrome mutation R200C, but not R79Q and Y86C, is essential for the**
600 **ciliogenesis function of ARL13B.** (**a**) The schematic diagram illustrates the organization of
601 ARL13B and its three Joubert syndrome mutants. See the legend of Figure 4a. (**b-c**) The cellular
602 distribution, cilium localization, and ciliogenesis percentage of GFP-tagged Joubert syndrome
603 mutant $ARL13B^R$. The boxed region is enlarged at the lower left corner, and the scale bar
604 represents 10 μm. See the legend of Figure 4b, c. (**d**) The images acquired as described in (b-c)
605 were analyzed. n = 3 independent experiments with ≥ 30 cells analyzed in each. The error bar
606 represents the *mean* ± *standard deviation.*

607

608 **Figure 6**

609 **Hedgehog signaling is abolished in *ARL13B*-KO cells.** (**a**) SAG treatment increased the cilium
610 localization of SMO in RPE1 cells. RPE1 cells treated with or without (control) 0.5 μM SAG for 24
611 hours were fixed and processed for immunofluorescence labeling of endogenous SMO and
612 ARL13B. Arrows and arrowheads indicate SMO-positive and -negative cilia, respectively. (**b**)
613 Percentage of ciliated cells with SMO-positive cilia. Images acquired as described in (a) were
614 analyzed. n = 4 independent experiments. (**c**) Normalized transcription levels of *SMO*, *PTCH1*,
615 and *GLI1* genes in parental RPE1 or sg1#a cells with or without (control) 0.5 μM SAG treatment
616 for 24 h. The transcription was quantified by qPCR and normalized by the corresponding control.
617 n = 5 independent experiments. (**d-e**) Exogenously expressed $ARL13B^R$-GFP can rescue the
618 SAG-induced cilium localization of SMO in *ARL13B*-KO cells. Parental RPE1 or sg1#a cells
619 expressing $ARL13B^R$-GFP were treated with or without (control) 0.5 μM SAG for 24 h. Cells were
620 subsequently fixed and processed for immunofluorescence labeling of endogenous SMO and
621 pericentrin (d). Arrows indicate ciliated cells. The percentage of $ARL13B^R$-GFP expressing ciliated
622 sg1#a cells with SMO-positive cilia is quantified in (e). n = 3 independent experiments with ≥ 100
623 cells analyzed in each. In (a, d), scale bar, 10 μm. In (b, c, e), the error bar represents the *mean*
624 ± *standard deviation,* and p-values were from unpaired, two-tailed t-tests. NS, $p > 0.05$; ∗, $p \leq$
625 0.05; ∗∗ $p \leq 0.005$; ∗∗∗ $p \leq 0.0005$.

626

Figure 1

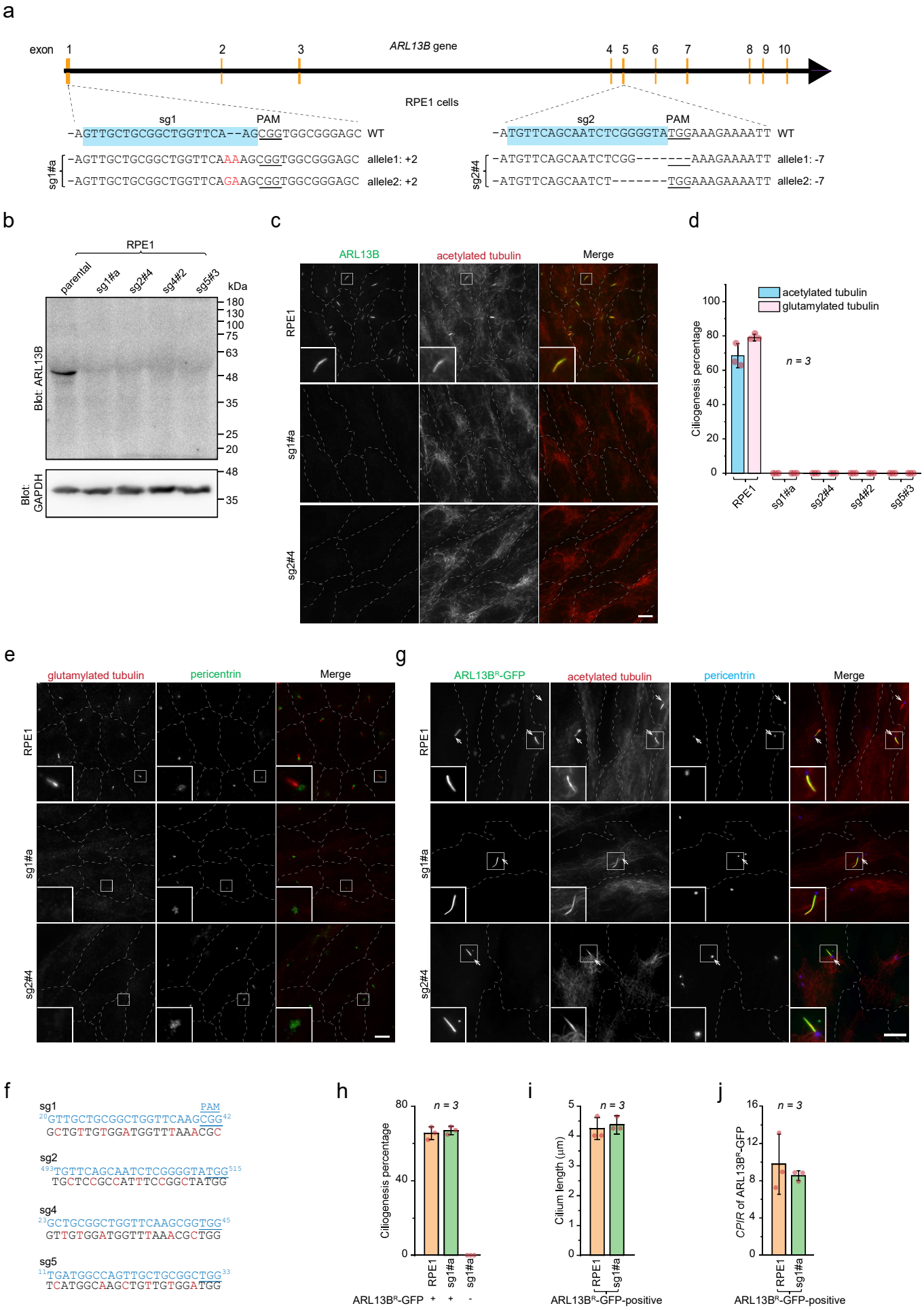
a
exon 1 2 3 4 5 6 7 8 9 10
ARL13B gene
RPE1 cells
sg1
PAM
-AGTTGCTGCGGCTGGTTCA--AGCGGTGGCGGGAGC WT
sg2
PAM
-ATGTTCAGCAATCTCGGGGTATGGAAAGAAAATT WT
sg1#a
-AGTTGCTGCGGCTGGTTCAAAAGCGGTGGCGGGAGC allele1: +2
-AGTTGCTGCGGCTGGTTCAGAAGCGGTGGCGGGAGC allele2: +2
sg2#4
-ATGTTCAGCAATCTCGG-------AAAGAAAATT allele1: -7
-ATGTTCAGCAATCT-------TGGAAAGAAAATT allele2: -7
b
RPE1
parental
sg1#a
sg2#4
sg4#2
sg5#3
kDa
180
130
100
75
63
48
35
25
20
Blot: ARL13B
Blot: GAPDH
48
35
c
ARL13B
acetylated tubulin
Merge
RPE1
sg1#a
sg2#4
d
acetylated tubulin
glutamylated tubulin
Ciliogenesis percentage
n = 3
RPE1
sg1#a
sg2#4
sg4#2
sg5#3
e
glutamylated tubulin
pericentrin
Merge
RPE1
sg1#a
sg2#4
g
ARL13BR-GFP
acetylated tubulin
pericentrin
Merge
RPE1
sg1#a
sg2#4
f
sg1
PAM
20GTTGCTGCGGCTGGTTCAAGCGG42
GCTGTTGTGGATGGTTTAAACGC
sg2
493TGTTCAGCAATCTCGGGGTATGG515
TGCTCCGCCATTTCCGGCTATGG
sg4
23GCTGCGGCTGGTTCAAGCGGTGG45
GTTGTGGATGGTTTAAACGCTGG
sg5
11TGATGGCCAGTTGCTGCGGCTGG33
TCATGGCAAGCTGTTGTGGATGG
h
Ciliogenesis percentage
n = 3
RPE1
sg1#a
sg1#a
ARL13BR-GFP + + -
i
Cilium length (μm)
n = 3
RPE1
sg1#a
ARL13BR-GFP-positive
j
CPIR of ARL13BR-GFP
n = 3
RPE1
sg1#a
ARL13BR-GFP-positive

Figure 2

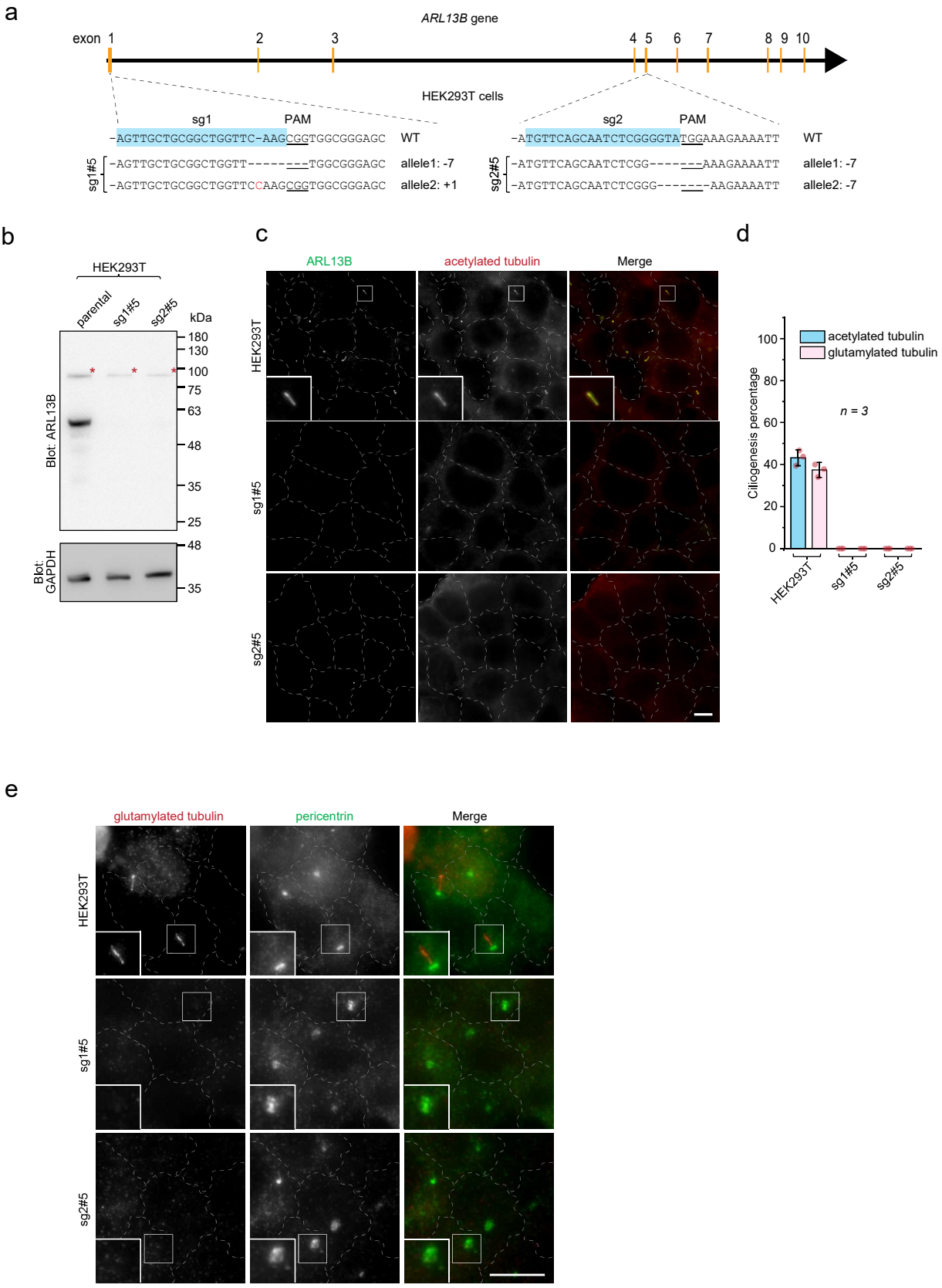
a
ARL13B gene
exon 1 2 3 4 5 6 7 8 9 10
HEK293T cells
sg1
PAM
-AGTTGCTGCGGCTGGTTC-AAGCGGTGGCGGGAGC WT
sg1#5
-AGTTGCTGCGGCTGGTT------TGGCGGGAGC allele1: -7
-AGTTGCTGCGGCTGGTTCCAAGCGGTGGCGGGAGC allele2: +1
sg2
PAM
-ATGTTCAGCAATCTCGGGGTATGGAAAGAAAATT WT
sg2#5
-ATGTTCAGCAATCTCGG-------AAAGAAAATT allele1: -7
-ATGTTCAGCAATCTCGGG------AAGAAAATT allele2: -7
b
HEK293T
parental
sg1#5
sg2#5
kDa
180
130
100
75
63
48
35
25
Blot: ARL13B
Blot: GAPDH
48
35
c
ARL13B
acetylated tubulin
Merge
HEK293T
sg1#5
sg2#5
d
acetylated tubulin
glutamylated tubulin
Ciliogenesis percentage
n = 3
100
80
60
40
20
0
HEK293T
sg1#5
sg2#5
e
glutamylated tubulin
pericentrin
Merge
HEK293T
sg1#5
sg2#5

Figure 3

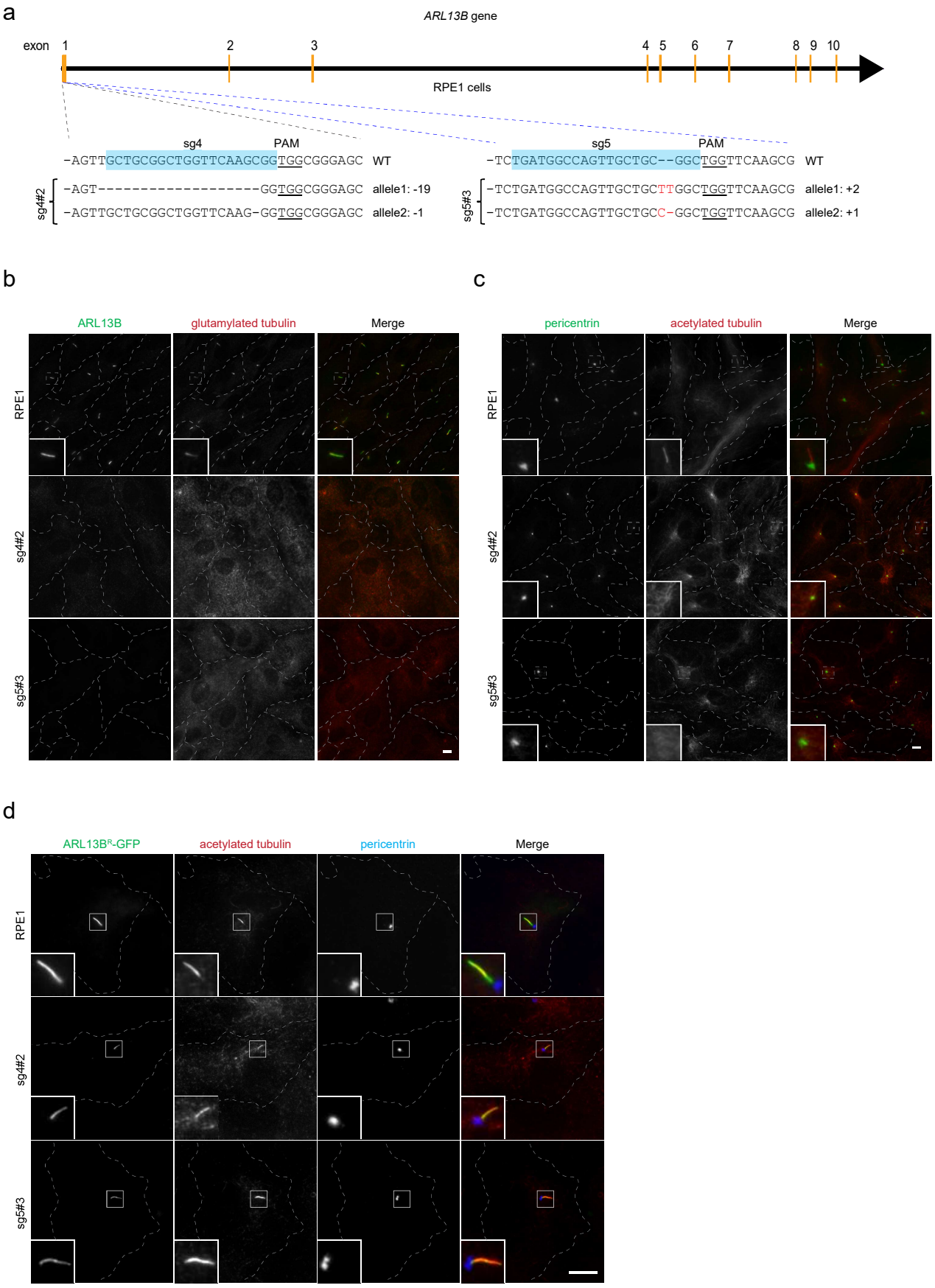
a
ARL13B gene
exon 1 2 3 4 5 6 7 8 9 10
RPE1 cells
sg4
PAM
-AGTTGCTGCGGCTGGTTCAAGCGGTGGCGGGAGC WT
sg4#2
-AGT----------GGTGGCGGGAGC allele1: -19
-AGTTGCTGCGGCTGGTTCAAG-GGTGGCGGGAGC allele2: -1
sg5
PAM
-TCTGATGGCCAGTTGCTGC--GGCTGGTTCAAGCG WT
sg5#3
-TCTGATGGCCAGTTGCTGCTTGGCTGGTTCAAGCG allele1: +2
-TCTGATGGCCAGTTGCTGCC-GGCTGGTTCAAGCG allele2: +1
b
ARL13B
glutamylated tubulin
Merge
RPE1
sg4#2
sg5#3
c
pericentrin
acetylated tubulin
Merge
RPE1
sg4#2
sg5#3
d
ARL13B^R-GFP
acetylated tubulin
pericentrin
Merge
RPE1
sg4#2
sg5#3

Figure 4

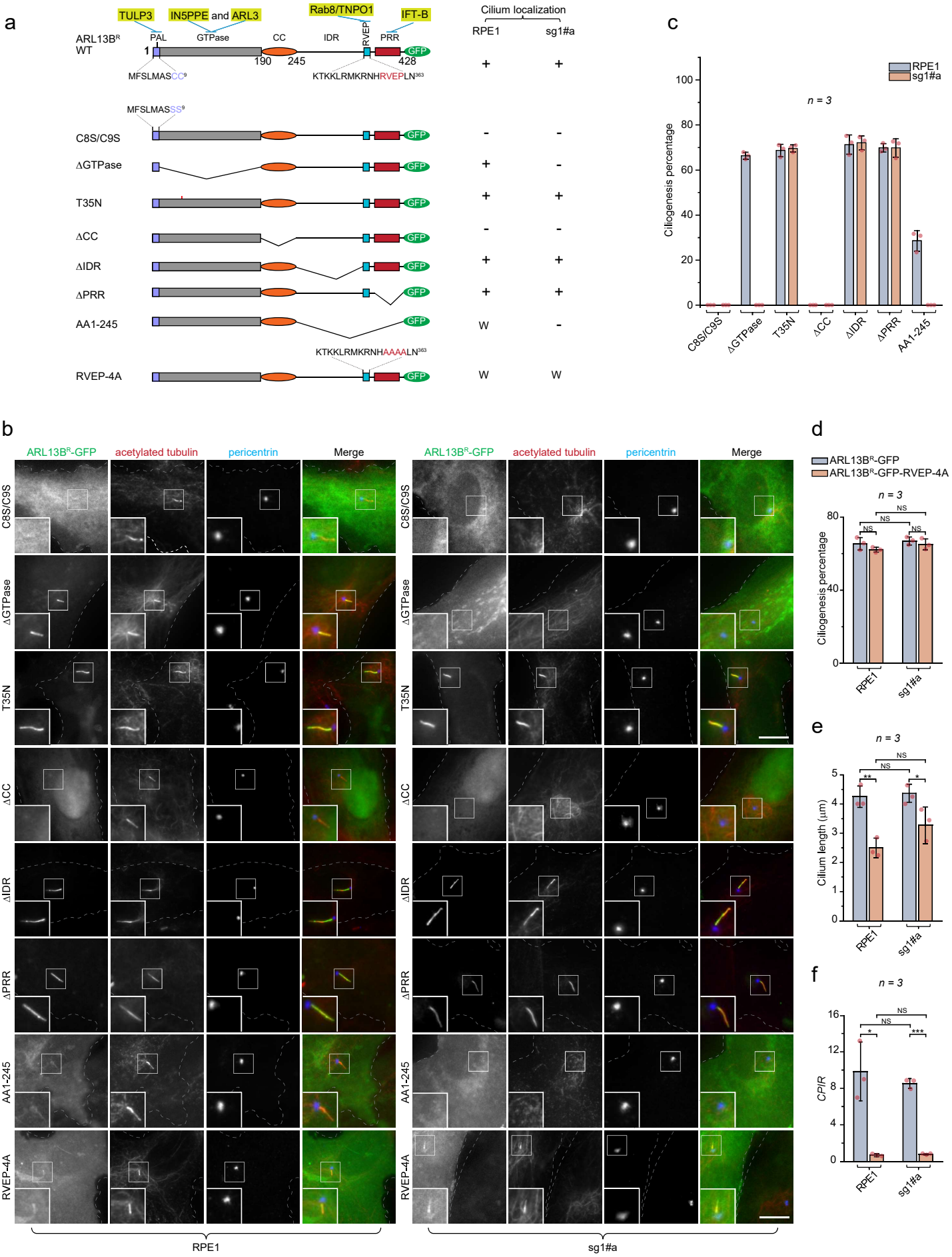
a
TULP3
IN5PPE and ARL3
Rab8/TNPO1
IFT-B
Cilium localization
RPE1
sg1#a
ARL13B^R WT
PAL
GTPase
CC
IDR
RVEP
PRR
GFP
1
190
245
428
MFSLMASCC9
KTKKLRMKRNHRVEPLN363
MFSLMASSS9
C8S/C9S
ΔGTPase
T35N
ΔCC
ΔIDR
ΔPRR
AA1-245
KTKKLRMKRNHAAAALN363
RVEP-4A
W
c
RPE1
sg1#a
n = 3
Ciliogenesis percentage
b
ARL13B^R-GFP
acetylated tubulin
pericentrin
Merge
d
ARL13B^R-GFP
ARL13B^R-GFP-RVEP-4A
NS
e
Cilium length (μm)
f
CPIR

Figure 5

a

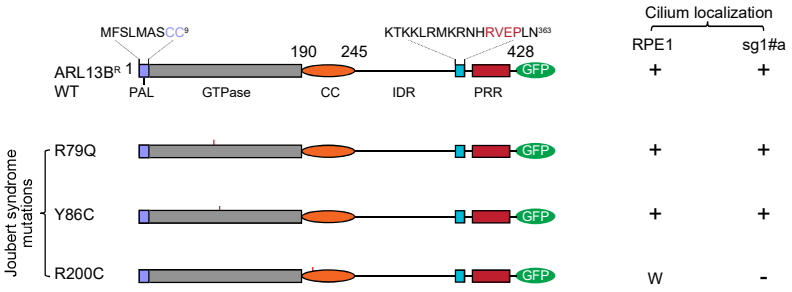

b

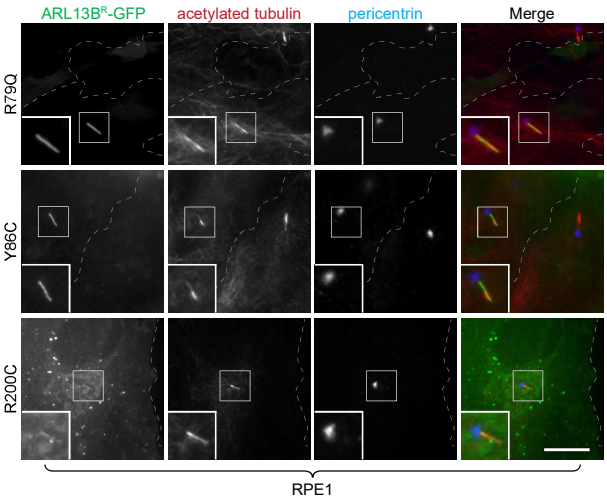

c

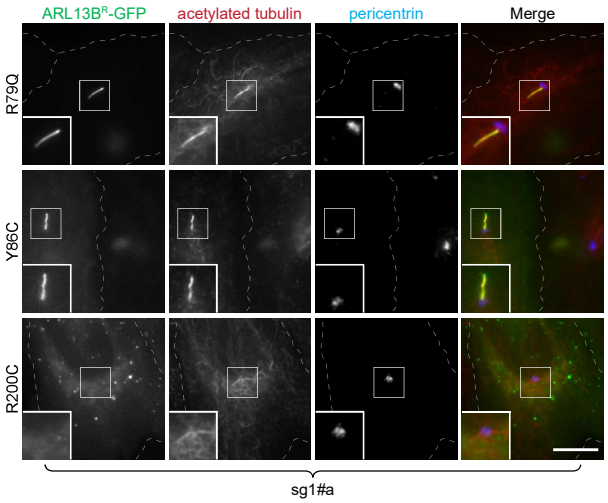

d

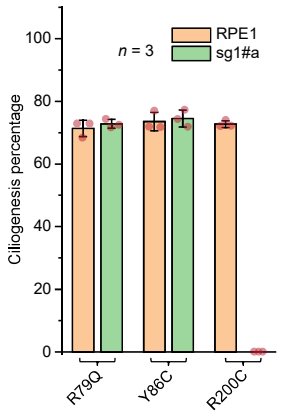

Figure 6

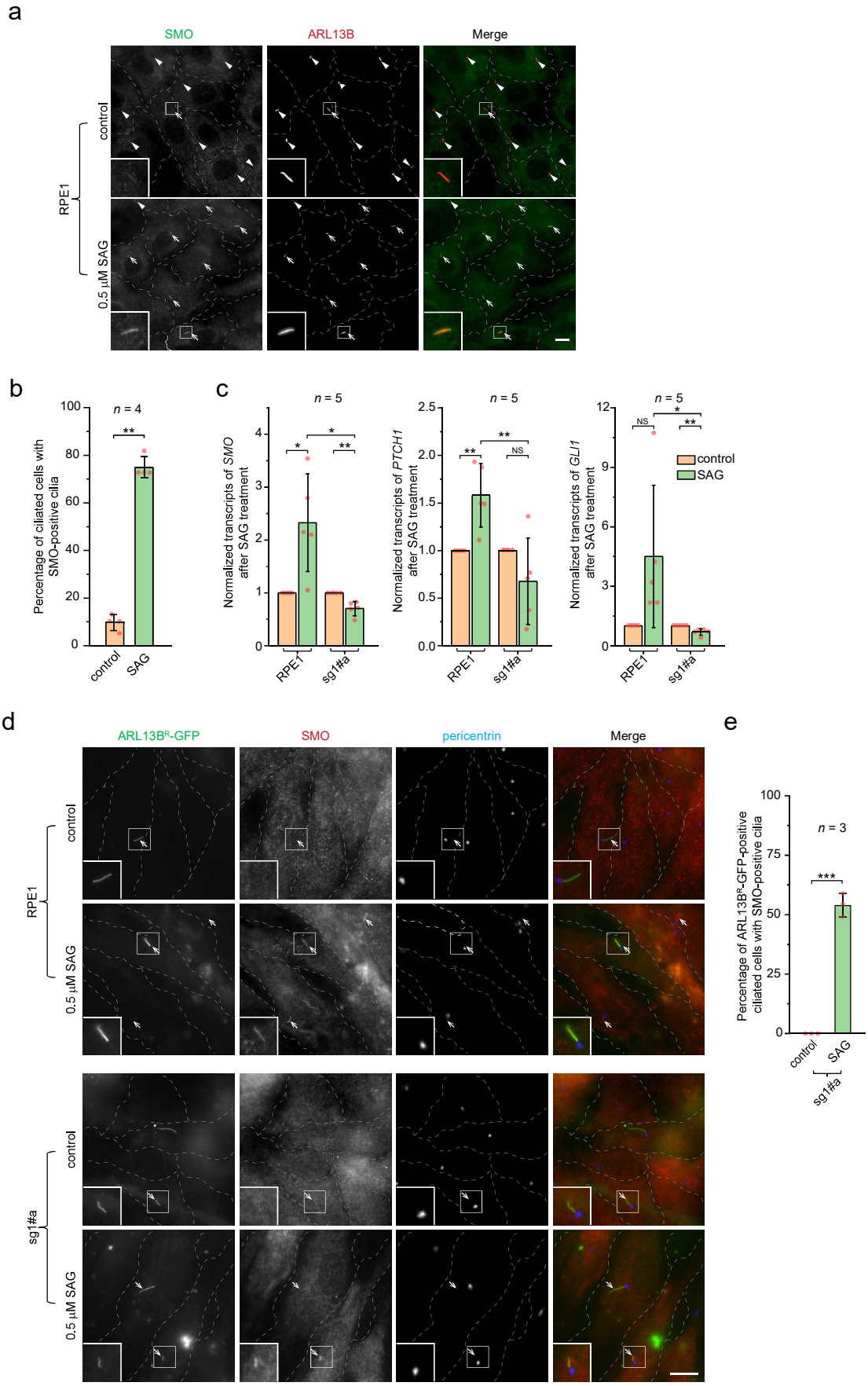
a
SMO
ARL13B
Merge
RPE1
control
0.5 μM SAG
b
n = 4
Percentage of ciliated cells with SMO-positive cilia
control
SAG
c
n = 5
Normalized transcripts of SMO after SAG treatment
Normalized transcripts of PTCH1 after SAG treatment
Normalized transcripts of GLI1 after SAG treatment
RPE1
sg1#a
NS
control
SAG
d
ARL13B^R-GFP
SMO
pericentrin
Merge
RPE1
control
0.5 μM SAG
sg1#a
e
n = 3
Percentage of ARL13B^R-GFP-positive ciliated cells with SMO-positive cilia
control
SAG
sg1#a